Numerical analysis of Swiss roll metamaterials

2009 J. Phys.: Condens. Matter 21 326006

(http://iopscience.iop.org/0953-8984/21/32/326006)

J. Phys.: Condens. Matter **21** (2009) 326006 (9pp) doi:10.1088/0953-8984/21/32/326006

Numerical analysis of Swiss roll metamaterials

A Demetriadou and J B Pendry

The Blackett Laboratory, Imperial College London, London SW7 2AZ, UK

E-mail: ademetri@imperial.ac.uk and j.pendry@imperial.ac.uk

Received 6 March 2009, in final form 25 June 2009
Published 23 July 2009
Online at stacks.iop.org/JPhysCM/21/326006

Abstract
A Swiss roll metamaterial is a resonant magnetic medium, with a negative magnetic permeability for a range of frequencies, due to its self-inductance and self-capacitance components. In this paper, we discuss the band structure, *S*-parameters and effective electromagnetic parameters of Swiss roll metamaterials, with both analytical and numerical results, which show an exceptional convergence.

(Some figures in this article are in colour only in the electronic version)

1. Introduction

All materials in nature are composites, consisted from atoms and molecules, which determine the electromagnetic properties of a material [1]. Based on this idea a new class of artificial materials, 'metamaterials', were developed whose subunits are of a smaller size than the wavelength of incident wave. Therefore, the wave is too myopic to see the individual geometry of subunits and consequently metamaterials can be characterized as homogeneous media, with effective electric permittivity (ε_{eff}) and magnetic permeability (μ_{eff}). The electromagnetic behaviour of metamaterials is governed by the subunit geometry and therefore, media can be constructed with novel electromagnetic properties, some of which are not seen in nature. One of the most fascinating is negative refraction, that can be realized when both the ε_{eff} and μ_{eff} of a medium are negative, as Veselago first noted [2]:

$$n = \begin{cases} +\sqrt{\varepsilon\mu} & \text{for } \varepsilon > 0 \text{ and } \mu > 0 \\ -\sqrt{\varepsilon\mu} & \text{for } \varepsilon < 0 \text{ and } \mu < 0. \end{cases} \quad (1)$$

There are various ways with which negative refraction can be realized. Metamaterials with both ε and μ resonant are most commonly called doubly negative metamaterials, since they require two different resonant structures to be brought together, in order to achieve negative refraction. The most well-known doubly negative metamaterial arises from the combination of a wire-mesh [3–5] and split-ring resonators [1], which was firstly constructed and tested experimentally for microwave frequencies by Smith *et al* [6]. Another interesting property, apart from negative refraction, is that metamaterials can be constructed with macroscopic magnetic behaviour, although their subunits are made entirely from conductors [1]. It is remarkable that the magnetic behaviour of metamaterials holds for frequencies where the magnetic response of conventional materials disappear (even for GHz frequencies). The majority of metamaterial community has focused on split-ring resonators, since they can be used with less difficulty in combination with the wire-mesh metamaterial and operate at higher frequencies, compared with Swiss rolls. However, Swiss rolls have different and equally interesting applications. Furthermore, by adding chiral inclusions in a resonant medium, a negative refractive band can be obtained for one wave polarization as described in [7, 8]. Therefore, a chiral Swiss roll metamaterial can be constructed, that achieves negative refraction with a continuous transition from the negative to positive band, for one wave polarization. In this paper, we investigate the behaviour of the simpler case of non-chiral Swiss roll metamaterials, numerically and compare it to analytical work [1] since, to the best of our knowledge, there is no numerical investigation due to design complexity and difficulties on modelling the structure.

Pendry *et al* [1] proposed that Swiss rolls and split-ring resonators made from thin conducting sheets, have a macroscopic magnetic behaviour for a magnetic field (H_0) applied along the rod. The magnetic field induces currents on the circumference of the cylinder and consequently a magnetization (i.e. electromotive force—emf) opposing the applied magnetic field [1, 9]. Therefore, it macroscopically appears that 'magnetic' monopoles are flowing up and down the cylinders (i.e. the magnetic equivalent of conducting wires). The capacitive and conductive elements of the structure

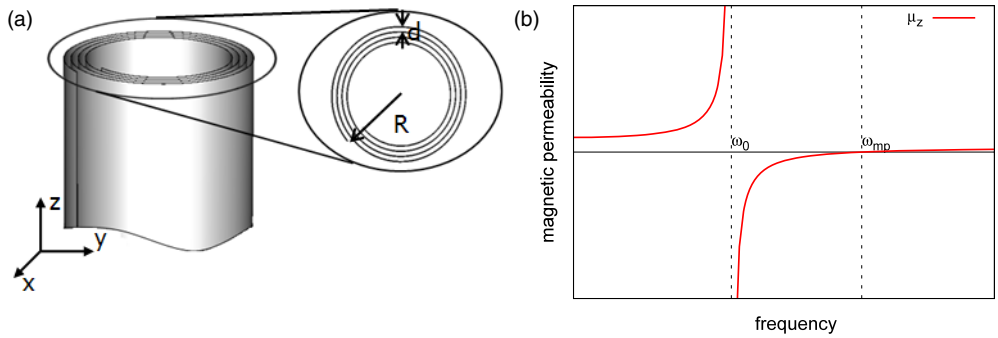

Figure 1. (a) A Swiss roll, where R is the outer radius, d the gap between the conducting sheets. (b) For magnetic fields along the Swiss roll, the metamaterial has an effective resonant magnetic permeability (μ_z). Note that $\mu_z < 0$ for $\omega_0 < \omega < \omega_{\rm mp}$.

create a resonant LC circuit that the induced currents are subjected to and therefore a resonant μ that takes negative values for a range of frequencies is achieved [1]. A Swiss roll resonator is made from a thin conducting sheet wrapped around a cylindrical mandrel in a spiral shape (figure 1). For a metamaterial consisted from Swiss rolls in a square lattice, the fields will obey:

$$\begin{aligned} \mathbf{D} &= \boldsymbol{\varepsilon}_{\rm eff}\varepsilon_0\mathbf{E} - {\rm i}\sqrt{\varepsilon_0\mu_0}\boldsymbol{\kappa}\mathbf{H} \\ \mathbf{B} &= \boldsymbol{\mu}_{\rm eff}\mu_0\mathbf{H} + {\rm i}\sqrt{\varepsilon_0\mu_0}\boldsymbol{\kappa}^{\rm T}\mathbf{E} \end{aligned} \tag{2}$$

where $\boldsymbol{\varepsilon}_{\rm eff}$ and $\boldsymbol{\mu}_{\rm eff}$ are the effective electric permittivity and magnetic permeability respectively, $\boldsymbol{\kappa}$ is the magnetoelectric coupling term that takes into account the bianisotropic nature of the structure. The currents induced on the spiral conducting sheet, because of the applied magnetic field oscillating along the Swiss roll, are dependent on radius R and the differential capacitance across d. Therefore, the effective magnetic permeability along the roll is plotted in figure 1(b) and given by [1]:

$$\begin{aligned} \mu_z^{\rm eff} &= 1 - \frac{(\pi R^2/a^2)\omega^2}{\omega^2 - \frac{{\rm d}c_0^2}{2\pi^2R^3\varepsilon_{\rm d}(N-1)} + \frac{{\rm i}2\rho\omega}{\mu_0 R(N-1)}} \\ &= 1 - \frac{F\omega^2}{\omega^2 - \omega_0^2 + {\rm i}\Gamma\omega} \end{aligned} \tag{3}$$

where ω is the frequency of the wave, $F = \pi R^2/a^2$ the filling factor, $\Gamma = 2\rho/[\mu_0 R(N-1)]$ accounts for the resistivity losses of the conducting material, ρ is the resistance of the conducting sheet per unit area and ω_0 the resonance frequency, which is given by [1]:

$$\omega_0 = c_0\sqrt{\frac{d}{2\pi^2R^3\varepsilon_{\rm d}(N-1)}} = \sqrt{\frac{1}{2\pi^2R^3\mu_0C(N-1)^2}} \tag{4}$$

where

$$C = \frac{\varepsilon_{\rm d}\varepsilon_0}{d(N-1)} = \frac{\varepsilon_{\rm d}}{\mu_0c_0^2d(N-1)}$$

is the capacitance of the system, $\varepsilon_{\rm d}$ the dielectric permittivity of the material in the gap between the conducting sheets, which we will assume to be vacuum (i.e. $\varepsilon_{\rm d} = 1$). The $\mu_z^{\rm eff}$ (1(b)) goes to infinity at ω_0 and to zero at $\omega_{\rm mp}$ (i.e. the 'magnetic' plasma frequency), which is given by [1]:

$$\begin{aligned} \omega_{\rm mp} &= c_0\sqrt{\frac{d}{(1-F)2\pi^2R^3\varepsilon(N-1)}} \\ &= \sqrt{\frac{1}{F2\pi^2R^3\mu_0C(N-1)^2}} = \frac{\omega_0}{\sqrt{1-F}}. \end{aligned} \tag{5}$$

In order to derive (3) we assumed that the conducting sheet is infinitely thin and that the radius of the Swiss roll is much larger than d (i.e. $R \gg d$).

The z-component of the electric permittivity can be found by considering an oscillating E_z-field along the Swiss rolls. In this case and for the long wavelength limit, the field would see thick conducting wires and therefore, the electric permittivity along the Swiss rolls (i.e. $\varepsilon_z^{\rm eff}$) obeys Drude's model:

$$\varepsilon_z^{\rm eff} = 1 - \frac{\omega_{\rm p}^2}{\omega^2} \tag{6}$$

where $\omega_{\rm p}$ is the plasma frequency, which takes values much higher than ω_0 and $\omega_{\rm mp}$ (i.e. $\omega_{\rm p} \gg \omega_0$ and $\omega_{\rm p} \gg \omega_{\rm mp}$), since for conducting wires as R increases $\omega_{\rm p}$ increases as well [10, 11]. Therefore, ε_z is negative for $\omega < \omega_{\rm p}$ [3–5]. This means that for k_x-propagation the band structure will not be doubly degenerate, since the mode with (E_z, H_y) fields is forbidden. Only the (E_y, H_z) mode will propagate.

Now, if we assume lateral electric or magnetic fields (i.e. in the x–y plane) and neglect the resistivity losses of the conducting sheet, then the lateral components of $\varepsilon_{\rm eff}$ and $\mu_{\rm eff}$ can be considered to be approximately constants [1]. The magnetic lines cannot penetrate the rods, and are constrained in the free space around the Swiss rolls, giving a spatially non-uniform magnetic field, resulting to $\mu_x^{\rm eff}$ and $\mu_y^{\rm eff}$ to take values [12–14]:

$$\mu_x^{\rm eff} = \mu_y^{\rm eff} \simeq \frac{\sqrt{1-F}}{2}. \tag{7}$$

Similarly, for the x- and y-components of the electric permittivity:

$$\varepsilon_x^{\rm eff} = \varepsilon_y^{\rm eff} \simeq \frac{2}{\sqrt{1-F}}. \tag{8}$$

Finally, due to the bianisotropic nature of the structure, a resonant magnetoelectric coupling term (κ) has to be

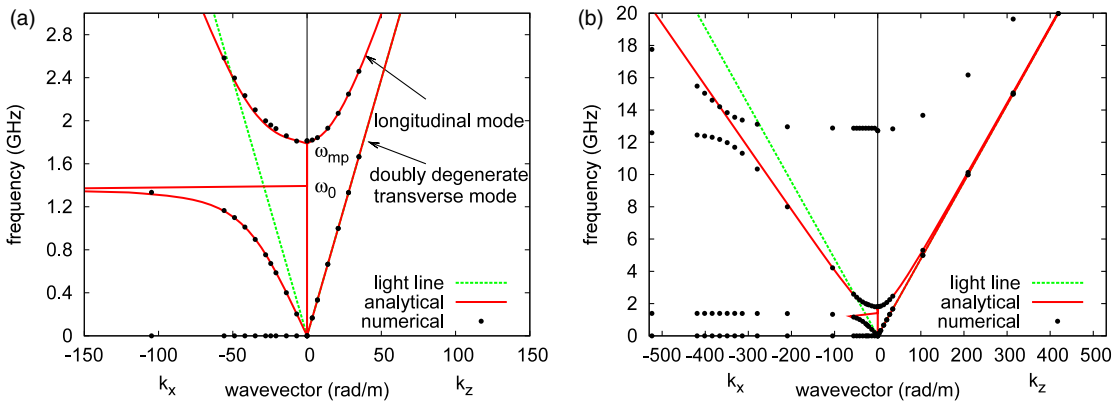

Figure 2. The analytical prediction (red solid line), plotted with numerical results (dots) for a Swiss roll metamaterial with dimensions $N = 2$, $d = 0.1$ mm, $x = 0.05$ mm, $R = 2$ mm and $a = 5$ mm. Note that the left part of both plots is the band structure for k_x-propagation and the right part for k_z-propagation. The light line is plotted with a green dashed line. (a) For $k \to 0$. Note that there is a stop band for $\omega_0 < \omega < \omega_{mp}$ and k_x-propagation, where $\mu_z < 0$. (b) At higher frequencies, the excitation of the first waveguide mode can be seen.

considered, which rakes the form:

$$\kappa_{yz} = \frac{\delta\omega\omega_0^2}{\omega^2 - \omega_0^2} \tag{9}$$

where δ is a constant.

2. Band structure

The dispersion equation for a medium consisted from Swiss rolls in a square lattice and aligned with the z-axes can be found considering Maxwell's equations for a monochromatic wave with frequency ω and wavevector $\mathbf{k}$. For simplicity, we assume that $k_y = 0$, and since we know that the medium is magnetically active and electrically inactive (for fields along the roll), Maxwell's equation can be rearranged in terms of $\mathbf{B}$, giving the dispersion equation [15]:

$$\omega = c_0\sqrt{\frac{k_x^2}{\varepsilon_y\mu_z} + \frac{k_z^2}{\varepsilon_y\mu_x}} \tag{10}$$

which is plotted in figure 2(a) (red line) for k_x-(left) and k_z-propagation (right). For k_x-propagation and frequencies $\omega_0 < \omega < \omega_{mp}$, the medium is opaque since $\mu_z^{eff} < 0$ and $\varepsilon_y^{eff} > 0$, introducing a stop band in the dispersion diagram. Also, the band structure is not doubly degenerate for k_x-propagation as expected, since the (E_z, H_y) mode is forbidden for $\omega < \omega_p$. Furthermore, in figure 2(a) (right) the band structure for k_z propagation is plotted as well. Now the electric and magnetic fields are in the x–y plane and therefore there are two doubly degenerate transverse modes (since $\varepsilon_x = \varepsilon_y$ and $\mu_x = \mu_y$), that are also degenerate with the light line ($\sqrt{\varepsilon_x\mu_y} = \sqrt{\varepsilon_y\mu_x} = 1$) as can be obtained from (7) and (8).

The Swiss roll is a rather complex design to be modelled for numerical calculations, since it is constructed from a thin conducting sheet arranged in a spiral shape with a relatively big radius and a small d [15, 16]. The fine details of the structure demand a huge computational power and time for adequate numerical accuracy. A way to go around this problem is to calculate the band structure for a Swiss roll with less fine detail (i.e. thicker conducting sheet and a smaller ratio of (R/d)). Therefore, the band structure of a Swiss roll with dimensions $x = 0.05$ mm, $d = 0.1$ mm, $R = 2$ mm, $a = 5$ mm and $N = 2$ (where x is the thickness of the conducting sheet), was numerically calculated using CST Microwave Studio[1] and plotted in figure 2(a) (black dots) with the analytical prediction (red solid lines) of (10). The analytical and numerical results show a significant agreement (i.e. ∼90%), even though some of the assumptions taken for the analytical work are not valid for the structure studied numerically (i.e. $x \to 0$ and $R \gg d$).

Figure 2(b) shows the band structure at higher frequencies, where the numerical calculations find equally-spaced flat modes. By carefully studying the H-fields (shown in figures 3(c) and (d)), these modes can be identified as trapped modes between the conducting sheet, (i.e. inside the spiral gap) which is acting as a spiral waveguide. The waveguide modes are observed at frequencies:

$$\omega_g^n = c_0\sqrt{k_{mp}^2 + \left(\frac{n\pi}{S}\right)^2 + k_z^2} \tag{11}$$

where n is a positive integer, k_{mp} is the wavevector associated with the'magnetic plasma' frequency in (5) and S is the length of the spiral waveguide given by:

$$S = \int_0^{2\pi(N-1)} \sqrt{\rho^2 + \left(\frac{\mathrm{d}\rho}{\mathrm{d}\theta}\right)^2}\,\mathrm{d}\theta \tag{12}$$

where ρ is the radius of the spiral waveguide and θ the angle created between ρ and $\rho = r_0$ (the inner radius of the conducting sheet). As N increases, the length of the spiral waveguide increases as well, leading to more dense waveguide modes. Numerical results agree with (11) approximately ∼95–96%, although the open boundary conditions were neglected and our results are consistent with [17].

However, as seen in figure 2(b) for k_x-propagation, the waveguide mode couples strongly with the transverse mode creating a band gap. It is expected that the stronger the

[1] CST GmbH, Darmstadt, Germany.

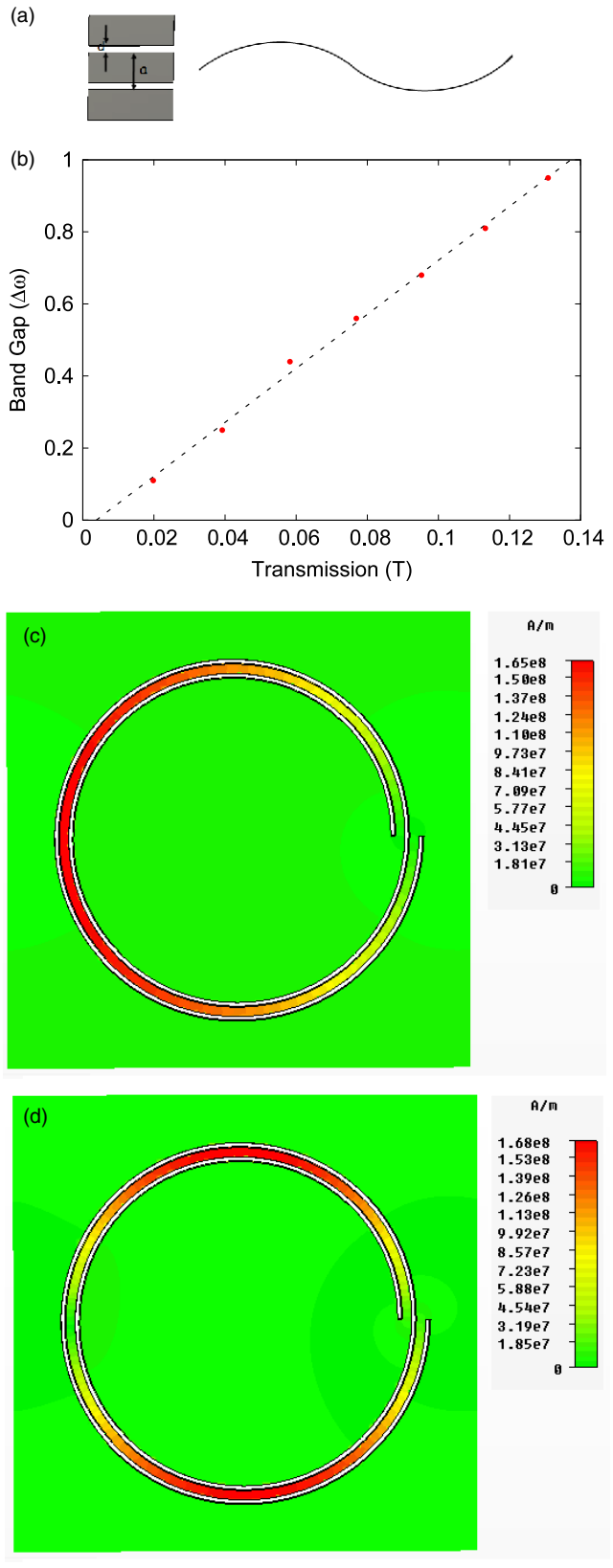

Figure 3. (a) A block-medium of periodicity a and gap between blocks d. (b) The band gap created due to the coupling of the waveguide and transverse modes is plotted, against the transmission of a wave through the block-medium (i.e. $T = \frac{2d}{d+a}$). (c) The magnetic field amplitude for the first waveguide mode and (d) the second waveguide mode.

coupling between the two modes, the bigger the band gap ($\Delta\omega$). A simple way to investigate this, is by considering the transmission of a wave through a medium consisted of blocks arranged in a square lattice of a and a gap between the blocks d, as shown in figure 3(a). The impedance of such a medium is given by $Z = (d/a)Z_0$, where Z_0 is the impedance of the hosting medium (i.e. vacuum), and by considering impedance matching at the interface, the transmission of the wave trapped in the waveguide is given by:

$$T = \frac{2Z}{Z + Z_0} = \frac{2d}{d + a} \tag{13}$$

$\Delta\omega$ was measured numerically for various Swiss rolls, and plotted in figure 3(b) against transmission ($T = \frac{2d}{d+a}$), and as expected they have a linear relationship. Therefore, for more fine dimensions of Swiss roll (i.e. smaller d) and where ω_0 is in MHz frequencies, the coupling between the waveguide and transverse modes is expected to be weak with a negligibly small band gap.

3. *S*-parameter calculations and effective parameter retrieval

For the Swiss roll metamaterial with band structure shown in figure 2, the *S*-parameters were calculated for normal incidence (i.e. k_x-propagation) on a 5-unit-cell slab with periodic boundary conditions in the y- and z-directions. Using the analytical predictions for the electromagnetic parameters in (3) and (8) and considering multiple scattering for a homogeneous slab as described in [18], the analytical prediction for the reflection coefficient is derived and plotted in figure 4 (red solid line) together with numerical results (blue dotted line). The agreement between the analytical and numerical results is significant and is ∼92% for frequencies up to 9 GHz, with a small difference on the value of ω_0, which is probably due to the approximations taken analytically and are not valid for the structure simulated here. At frequencies higher than 9 GHz the agreement breaks since the wavelength becomes comparable to lattice constant, therefore internal scattering within the unit cell takes place and the homogenization theory is not valid. Also, the excitation of the first waveguide mode can be seen in figure 4(a), and its value is in an agreement with (11) at ∼98%.

Although the scattering parameters show important information about the behaviour of a structure, it is usually preferable to obtain the effective electromagnetic parameters, which can be retrieved from the numerically calculated *S*-parameters. The methods that can be used for isotropic media are well documented in literature [19, 20], as well as for anisotropic media in [21] (such as wires combined with split-ring resonators). However, Chen *et al* [22] discuss ε and μ retrieval, specifically for bianisotropic media, accounting for the magnetoelectric coupling term. The S_{11} and S_{21}-parameters can be written as [19–22]:

$$S_{11} = \frac{r_{01}[1 - \exp(\mathrm{i}2nk_0ma)]}{1 - |r_{01}|^2 \exp(\mathrm{i}2nk_0ma)} \tag{14}$$

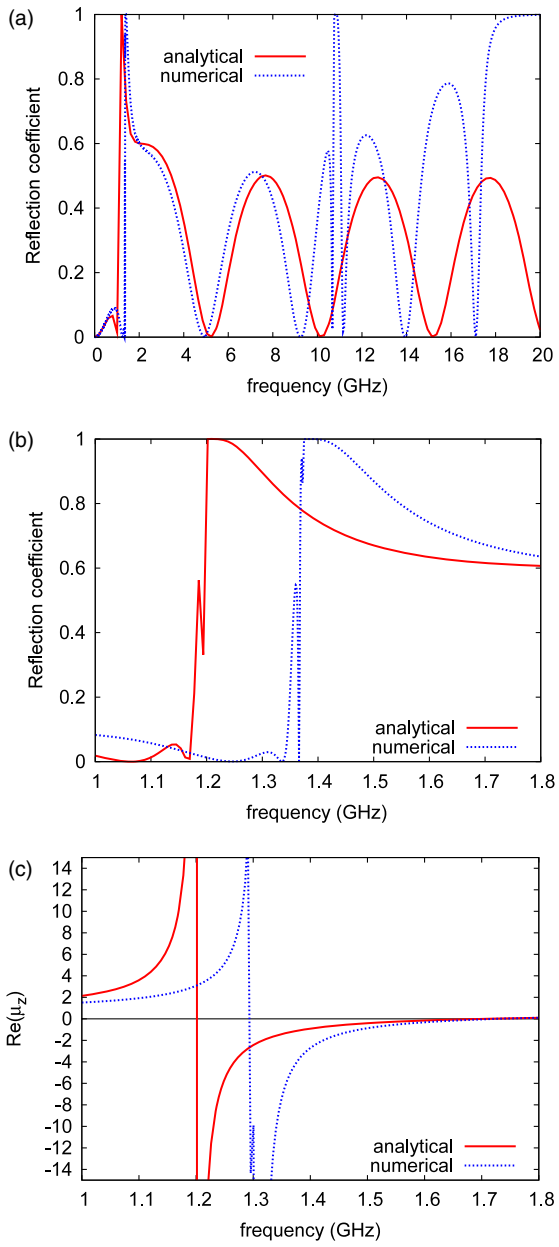

Figure 4. The analytic prediction (red solid line) and the numerical result (blue dotted line) for the reflection coefficient ($|R|$) is plotted for normal incidence on a five unit cell slab of a Swiss roll metamaterial with dimensions $N = 2$, $d = 0.1$ mm, $x = 0.05$ mm, $R = 2$ mm, $a = 5$ mm and band structure shown in figure 2. (a) For a wide frequency range, where the excitation of the first waveguide mode can be seen and (b) for $\omega \to \omega_o$. (c) The analytical prediction of μ_z shown in (3) (red solid line) plotted with μ_z retrieved from numerical results (blue dotted line).

$$S_{21} = \frac{(1 - |r_{01}|^2)\exp(ink_0ma)}{1 - |r_{01}|^2\exp(i2nk_0ma)} \tag{15}$$

where $r_{01} = (z-1)/(z+1)$ for vacuum impedance $z_0 = 1$, z the medium impedance, n the refractive index, k_0 the wavevector of the incident wave, m the number of unit cells in the slab, ma the width of the slab and by solving (14) and (15), the impedance and refractive index are obtained [22]:

$$z = \sqrt{\frac{DC'' - B'}{A'} - \frac{D^2}{4}} + i\frac{D}{2} \tag{16}$$

where

$$A = 2S_{11} - S_{11}^2 - 1 + S_{21}^2 \qquad B = 2S_{11} + S_{11}^2 + 1 - S_{21}^2$$
$$C = S_{11}^2 + S_{21}^2 - 1 \qquad D = \frac{A''B' - A'B''}{A''C'' + A'C'} \tag{17}$$

and $(\cdot)'$, $(\cdot)''$ denote the real and imaginary parts of the operators respectively and:

$$n = -\frac{i}{k_0 d}\ln\left(\frac{r_{01} - S_{11}}{S_{21}r_{01}}\right). \tag{18}$$

Therefore, the electric permittivity along the y-axis is given by:

$$\varepsilon_y = \frac{n - i\kappa}{z} \tag{19}$$

the magnetic permeability along the z-axis:

$$\mu_z = z(n + i\kappa) \tag{20}$$

and the magnetoelectric coupling by:

$$\kappa = \frac{1}{2i}\left(\frac{\mu_y}{z} - \varepsilon_y z\right). \tag{21}$$

Therefore, by applying the above formulae for the numerically calculated S-parameter shown in figure 4(b), the magnetic permeability is retrieved and plotted (blue dotted line) with the analytical prediction (red solid line) of (3) in figure 4(c). They both have the same shape with a terrific agreement (higher than 92%). This denotes that the modelling of a Swiss roll metamaterial as a medium with parameters given by (3) and (8) is a sufficiently accurate model. Furthermore, the real and imaginary parts of the retrieved $\varepsilon_y^{\text{eff}}$, μ_z^{eff}, refractive index (n) and the impedance (z) are shown in figure 5. It can be seen that both the impedance and refractive index real parts are always positive for the frequencies where the metamaterial is passive, and equal to zero for the stop band frequencies, as expected. Also, their imaginary parts have a sharp peak at resonance frequency.

Furthermore, the dependence of $\text{Re}(\mu_z)$ on the size of the gap between the conducting sheets (d) is investigated and is plotted in figure 6(a), where the expected behaviour from (3) and (4) is obtained. However, the analytical prediction depends on the validity of the assumption taken theoretically that $R \gg d$, which is clearly confirmed in figure 6(a). The disagreement is only on the value of ω_0 and reduces for higher values of (R/d). Also, the dependence of the dielectric constant (ε_d) of the material inside the gap is plotted in figure 6(b), where the behaviour is as expected from (4). The disagreement between analytical and numerical results is due to the value of d (i.e. $d = 0.1$ mm), where the contribution of various ε_d on the accuracy is almost negligible. Finally, in figure 6(c), the retrieved $\text{Re}(\mu_z)$ is plotted for various thicknesses of the conducting sheet and for $d = 0.1$ mm,

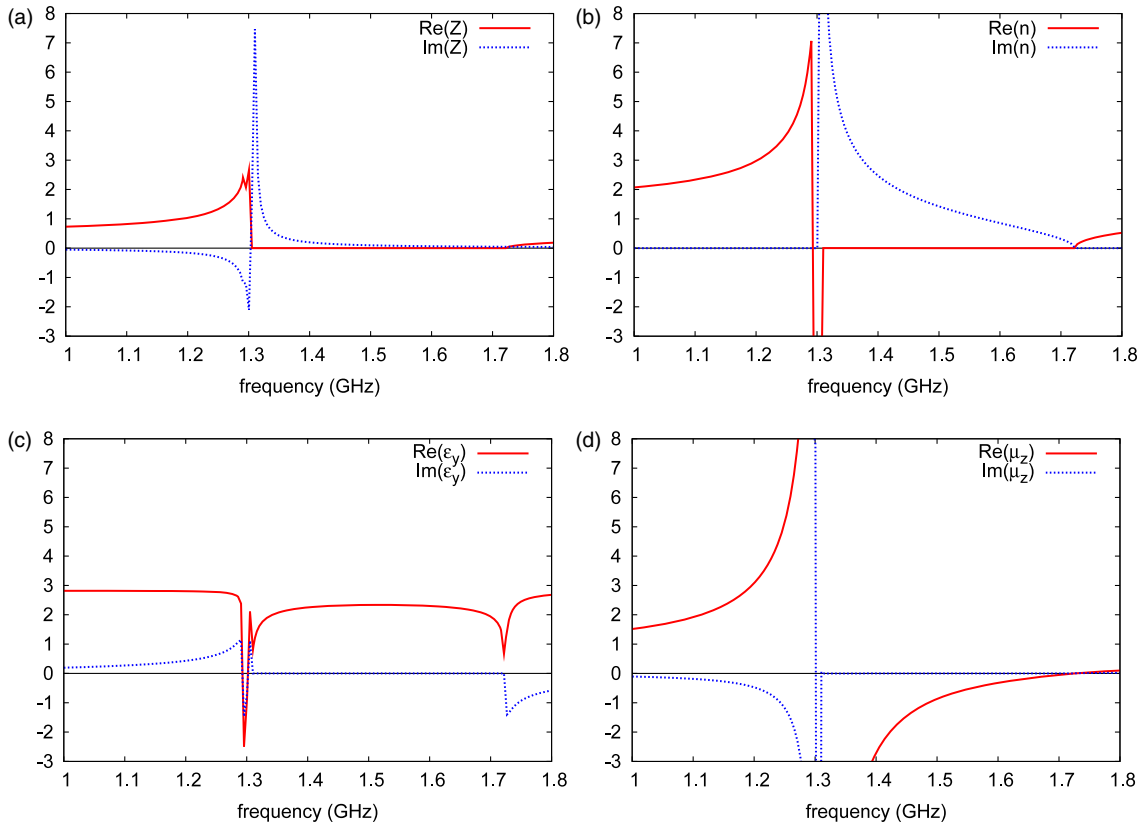

Figure 5. The retrieved effective electromagnetic parameters (z, n, ε, μ) from numerical S-parameter results of a Swiss roll metamaterial with dimensions $x = 0.05$ mm, $d = 0.1$ mm, $R = 2$ mm, $a = 5$ mm and $N = 2$. The electromagnetic parameters are plotted for $\omega \to \omega_0$ and the real parts are plotted with the red solid line and the imaginary part with the blue dotted line. (a) Impedance (Z), (b) refractive index (n), (c) electric permittivity (ε_y) across the Swiss roll and (d) the magnetic permeability (μ_z) along the roll.

$\varepsilon_d = 1$. As the conducting sheet becomes thinner, the value of ω_0 converges. However, the inaccuracy that a thicker conducting sheet induces to numerical results is minor (i.e. ∼3–5%), with respect to the extreme reduction on the demand of computational power.

4. Swiss roll metamaterials at MHz frequencies

Swiss roll metamaterials are most commonly used at MHz frequencies [15, 16, 23, 24], where they deploy an infinitely thin conducting sheet and $R \gg d$. Despite the tremendous modelling and computational problems of such a complicated structure, the S-parameters were numerically calculated for a Swiss roll metamaterial with dimensions $N = 5$, $x = 5$ μm, $d = 25$ μm, $R = 2500$ μm and $a = 7000$ μm. For normal incidence on a three-unit-cell slab, the numerical (blue dotted line) and analytical (red solid line) results for $|R|$ are plotted in figures 7(a) and (b), where the analytical prediction was derived in the same way described in section 3. The agreement between the analytical and simulation results is ∼95% for frequencies around ω_0. The S-parameters were also calculated numerically for a broader frequency range, where the excitation of the first and second waveguide modes can be seen as sharp resonances (figure 7(a)). The waveguide frequencies are also well predicted by (11), with an agreement of ∼99%. The retrieved μ_z^{eff} is plotted with the analytical prediction of (3), in figure 7(c). Both have the same behaviour, with a slight shift on the value of ω_0. Furthermore, the electromagnetic parameters retrieved from numerical S-parameter results are shown in figure 8. The real parts of the impedance and refractive index are always positive, or zero for frequencies where μ_z takes negative values. The main difference from the GHz structure is that ε_y has a weaker resonance, which agrees even more with the approximation taken in (8) that ε_y is approximately constant.

Finally, using the retrieved $\varepsilon_y^{\text{eff}}$ and μ_z^{eff} shown in figure 8 and the dispersion equations in (10), an estimate for the band structure for a Swiss roll metamaterial with dimensions $N = 5$, $x = 5$ μm, $d = 25$ μm, $R = 2500$ μm, $a = 7000$ μm was derived and plotted in figure 9, since it was not possible to derive it directly with numerical calculations. In figure 9(a), the band structure is plotted for $k_x \to 0$ and in figure 9(b), the first waveguide mode is shown as well. Also note that since d is smaller, the waveguide mode coupling with the transverse mode is considerably weaker, as expected.

The agreement between analytical and numerical results for a frequency range from few MHz to tenths of GHz is remarkable. An important advantage of Swiss rolls over other artificially magnetic media (such as split-ring-resonators), is the fact that their resonance frequency can be tune over a very broad frequency range by simply changing d (figure 6(a)) or ε_d (figure 6(c)) or R or a. Also, Swiss rolls have applications

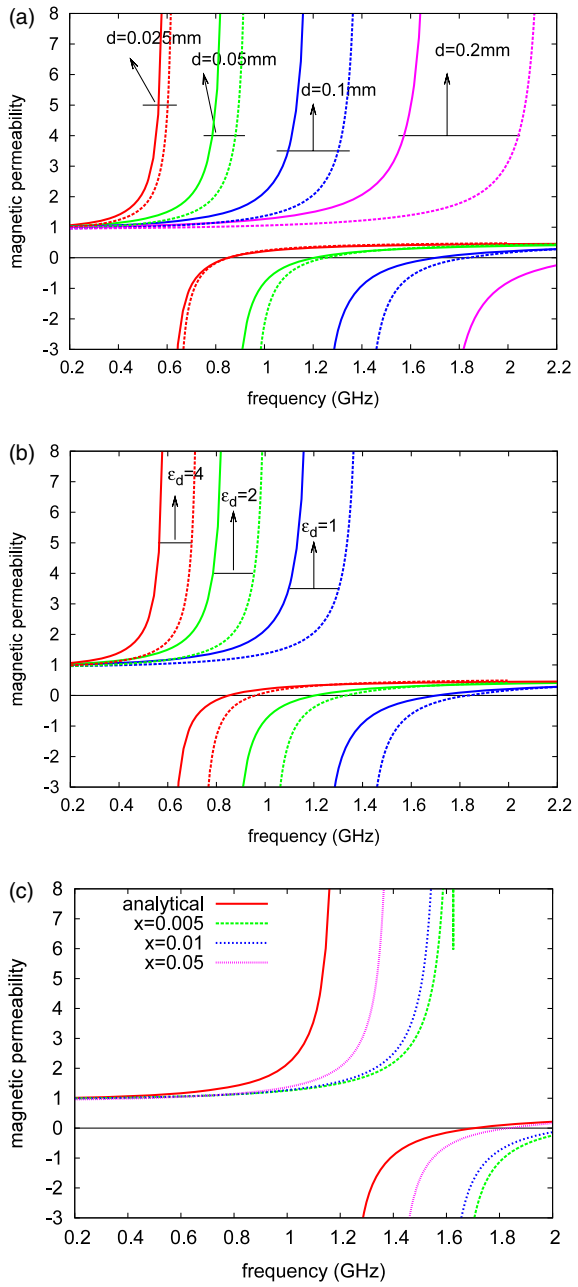

Figure 6. For Swiss rolls with radius $R = 2$ mm, lattice constant $a = 5$ mm and $N = 2$ (a) analytical (solid lines) and retrieved (dashed lines) $\mathrm{Re}(\mu_z)$ is plotted against frequency for various values of d (red: $d = 0.025$ mm, green: $d = 0.05$ mm, blue: $d = 0.1$ mm and pink: $d = 0.2$ mm) filled with vacuum (i.e. $\varepsilon_\mathrm{d} = 1$) and for $x = 0.05$ mm (b) analytical (solid lines) and retrieved (dashed lines) of $\mathrm{Re}(\mu_z)$ against frequency for various values of ε_d (red: $\varepsilon_\mathrm{d} = 4$, green: $\varepsilon_\mathrm{d} = 2$ and blue: $\varepsilon_\mathrm{d} = 1$) for $d = 0.1$ mm and $x = 0.05$ mm. (c) Analytical (solid lines) and retrieved (dashed lines) of $\mathrm{Re}(\mu_z)$ against frequency for various values of the conducting sheet's thickness x ($d = 0.1$ mm and $\varepsilon_\mathrm{d} = 1$).

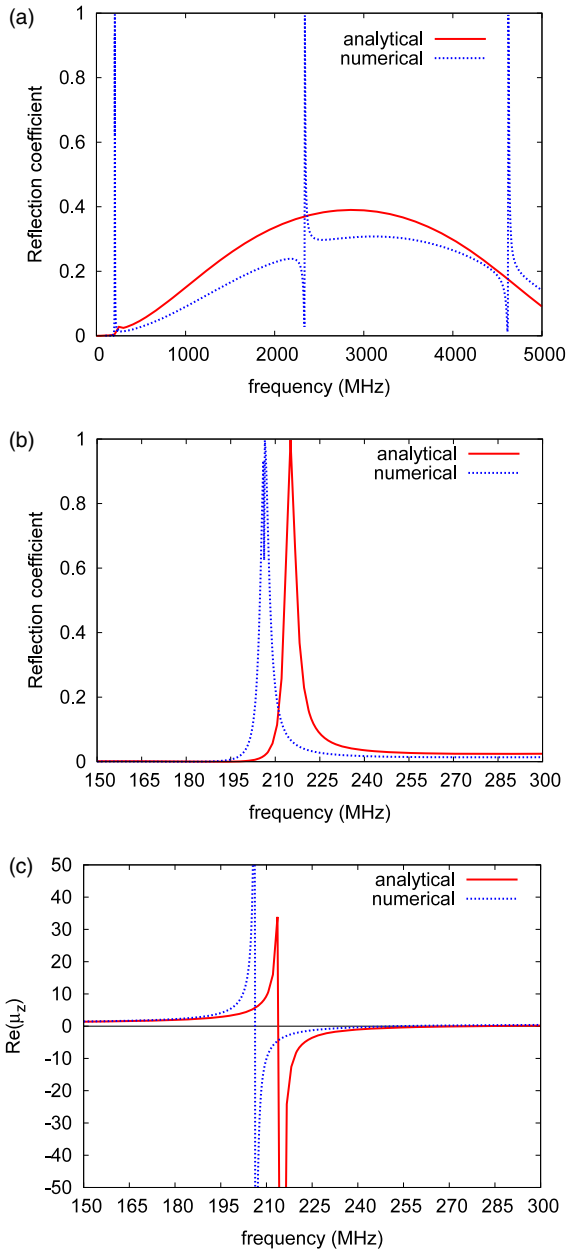

Figure 7. The analytic prediction (red solid line) and the numerical result (blue dotted line) for the reflection coefficient ($|R|$) is plotted for normal incidence on a five unit cell slab of a Swiss roll metamaterial with dimensions $N = 5$, $x = 5$ μm, $d = 25$ μm, $R = 2500$ μm and $a = 7000$ μm. (a) For a wide frequency range, where the excitation of the first two waveguide modes can be seen and (b) for $\omega \to \omega_o$. (c) The analytical prediction of μ_z shown in (3) (red solid line) plotted with μ_z retrieved from numerical results (blue dotted line).

that other magnetic metamaterials cannot be used or are not as efficient, like in magnetic resonance imaging (MRI) and some antenna applications.

The agreement between theory and numerical results is outstanding allowing us to move to the even more complicated structure, the chiral Swiss roll, firstly introduced in [7]. As discussed in [7, 8], the magnetic resonant behaviour of chiral Swiss rolls arises in the same way that it does for the non-chiral structures. Also, due to chirality and magnetic resonant behaviour, a negative band for one wave polarization is created. The extreme chirality and the negative band make chiral Swiss rolls suitable for various applications, such as polarization rotation or selection antennas and antennas where linear-to-circular wave transformation is necessary.

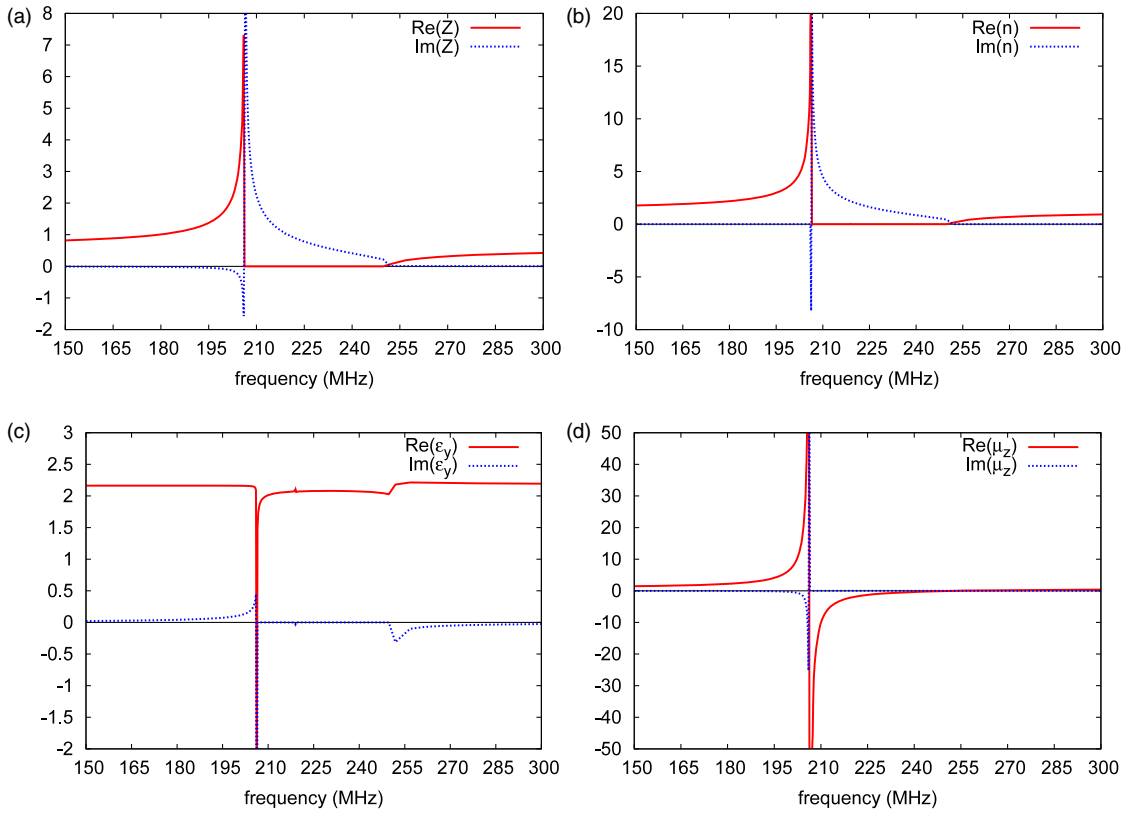

Figure 8. The retrieved effective electromagnetic parameters (z, n, ε, μ) from numerical S-parameter results of a Swiss roll metamaterial with dimensions $N = 5$, $x = 5$ μm, $d = 25$ μm, $R = 2500$ μm and $a = 7000$ μm. The electromagnetic parameters are plotted at $\omega \to \omega_0$ and the real parts with the red solid line and the imaginary part with the blue dotted line: (a) impedance (Z), (b) refractive index (n), (c) electric permittivity across the rolls (ε_y) and (d) magnetic permeability along the rolls (μ_z).

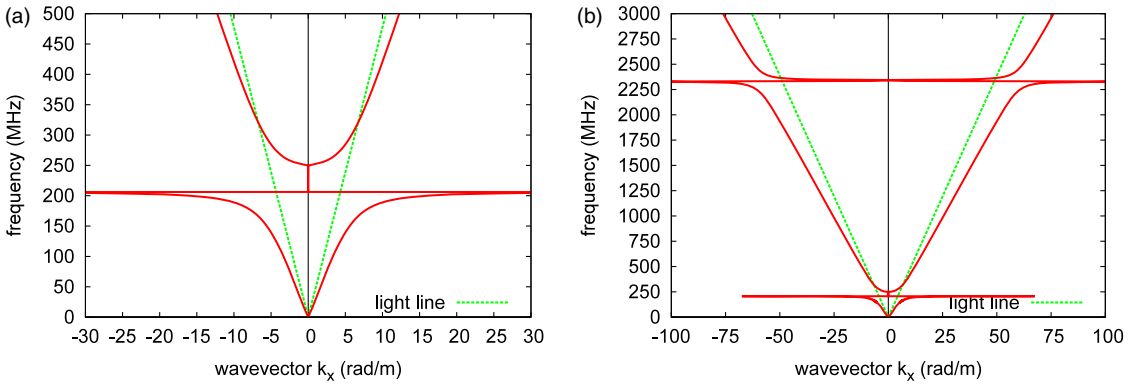

Figure 9. The band structure for k_x-propagation in a Swiss roll metamaterial with dimensions $N = 5$, $x = 5$ μm, $d = 25$ μm, $R = 2500$ μm and $a = 7000$ μm. (a) The band structure for $\omega \to \omega_0$ and (b) for a wide frequency range, where the first waveguide mode cam be seen.

5. Conclusions

An extensive numerical investigation of Swiss roll metamaterials was carried out, that seemed to be neglected from the community until now due to difficulties to numerically model such a complicated structure. We investigated the band structure, S-parameters and the effective electromagnetic parameters for a Swiss roll metamaterials operating in GHz frequencies, where an excellent agreement was found with analytical work. Some additional resonances were also found, that were identified as modes trapped inside the spiral gap created from the conducting sheet. Finally, for Swiss rolls with ω_0 at lower frequencies (MHz frequencies) an even higher agreement with analytical work was found and hence it can be concluded that the analytical homogenization model is exceptionally valid for Swiss rolls operating at a broad frequency range.

References

[1] Pendry J B, Holden A J, Robbins D J and Stewart W J 1999 Magnetism form conductors and enhanced nonlinear phenomena *IEEE Trans. Microw. Theory Tech.* **47** 2075

[2] Veselago V G 1968 The electrodynamics of substances with simultaneously negative values of ε and μ *Sov. Phys.—Usp.* **10** 509
[3] Pendry J B, Holden A J, Stewart W J and Young I 1996 Extremely low frequency plasmons in metallic mesostructures *Phys. Rev. Lett.* **76** 4773–6
[4] Pendry J B, Holden A J, Robbins D J and Stewart W J 1998 Low frequency plasmons in thin-wire structures *J. Phys.: Condens. Matter* **10** 4785–809
[5] Demetriadou A and Pendry J B 2008 Taming spatial dispersion in wire metamaterial *J. Phys.: Condens. Matter* **20** 295222
[6] Shelby R A, Smith D R and Schultz S 2001 Experimental verification of a negative index of refraction *Science* **292** 77–9
[7] Pendry J B 2004 A chiral route to negative refraction *Science* **306** 1353–5
[8] Demetriadou A and Pendry J B 2009 Extreme chirality in swiss roll metamaterials *J. Phys.: Condens. Matter* at press
[9] Ramakrishna S A 2005 Physics of negative refractive index materials *Rep. Prog. Phys.* **68** 449
[10] Belov P A, Tretyakov S A and Viitanen A 2002 Dispersion and reflection properties of artificial media formed by regular lattices of ideally conducting wires *J. Electromagn. Waves Appl.* **16** 1153–70
[11] Belov P A, Marques R, Maslovski S I, Nefedov I S, Silveirinha M, Simovski C R and Tretyakov S A 2003 Strong spatial dispersion in wire media in the very large wavelength limit *Phys. Rev.* B **67** 113103
[12] Wood B and Pendry J B 2007 Metamaterial at zero frequency *J. Phys.: Condens. Matter* **19** 076208
[13] Shurig D, Pendry J B and Smith D R 2006 Calculation of material properties and ray tracing in transformation media *Opt. Express* **14** 9794–804
[14] Smith D R and Pendry J B 2006 Homogenization of metamaterials by field averaging *J. Opt. Soc. Am.* B **23** 391
[15] Wiltshire M C K 2007 Radio frequency (rf) metamaterials *Phys. Status Solidi* **244** 1227–36
[16] Wiltshire M C K, Pendry J B, Williams W and Hajnal J V 2007 An effective medium description of 'swiss rolls', a magnetic metamaterial *J. Phys.: Condens. Matter* **18** L315–21
[17] Zolla F, Nicolet A and Guenneau S 2007 Swiss roll lattices: numerical and asymptotic modeling *Waves Random Complex Media* **17** 571–9
[18] Pendry J B 2000 Negative refraction makes a perfect lens *Phys. Rev. Lett.* **85** 3966–9
[19] Smith D R, Schultz S, Markos P and Soukoulis C M 2002 Determination of effective permittivity and permeability of metamaterials from reflection and trasmission coefficients *Phys. Rev.* B **65** 195104
[20] Chen X, Grzegorczyk T M, Wu B I, Pacheco J and Kong J A 2004 Robust method to retreive the constitute effective parameters of metamaterials *Phys. Rev.* E **70** 016608
[21] Smith D R, Vier D C, Koschny T and Soukoulis C M 2005 Electromagnetic parameter retrieval from inhomogeneous metamaterials *Phys. Rev.* E **71** 036617
[22] Chen X, Wu B I, Kong J A and Grzegorczyk T M 2005 Retrieval of the effective constitutive parameters of bianisotropic metamaterial *Phys. Rev.* E **71** 046610
[23] Wiltshire M C K, Pendry J B and Hajnal J V 2006 Sub-wavelength imaging at radio frequency *J. Phys.: Condens. Matter* **19** 456216
[24] Wiltshire M C K, Hajnal J V, Pendry J B, Edwards D J and Stevens C J 2003 Metamaterial endoscope for magnetic field transfer: near field imaging with magnetic wires *Opt. Express* **11** 709–15